Microstructure and Magnetic Properties of Fe-doped MnBi Permanent Magnet Alloys

Yuan-Hao Tu[1,2], Qiong Wu[1]*, Hong-Liang Ge[1], Zi-Sheng Wang[1], Min-Xiang Pan[1], and Yu Zhao[2]

[1]*Magnetism Key Laboratory of Zhejiang Province, China Jiliang University, Hangzhou 310018, China*
[2]*Hangzhou Permanent Magnet Group Co., LTD., Hangzhou 311231, China*

The melt-spinning method combined with annealing technology was used to prepare Mn-based permanent alloys in the paper. The influences of Fe-doping on the microstructure and magnetic performances of the MnBi alloys were studied. According to the results of XRD pattern, the fraction of the LTP-MnBi in the as spun MnBi ribbons increases with the doping of Fe element, a significant increase of the LTP-MnBi is due to annealing treatment. The magnetization at the 20 kOe field of $Mn_{55}Bi_{40}Fe_5$ melt-spun ribbons increases to 45 emu/g after being annealing. With the addition of Fe, the coercivity H_{cj} of the annealed ribbons increases first and then decreases. The results of δM plots show that the reduction of H_{cj} for the $Mn_{55}Bi_{40}Fe_5$ melt-spun ribbons can be attributed to enhanced exchange coupling interaction between MnBi LTP particles. The grain refinement contributes directly to an enhanced exchange coupling for the addition of 5 at% Fe from TEM images. The dependence of coercivity on temperature for the annealed MnBi alloy melt-spun ribbons is discussed.

Keywords : MnBi permanent alloys, Fe-doped, Magnetic properties

1. Introduction

As is well known, MnBi-based alloys possess optimal low-temperature intermetallic phase (LTP) with attractive uniaxial magnetocrystalline anisotropy and positive temperature coefficient which are considered as a kind of significant and potential materials to replace rare earth permanent magnet [1-3]. Their cost of unit energy product is significantly reduced compared with the well-known NdFeB-based magnets, especially in high temperature environment [4, 5]. Unfortunately, it is far from easy to get a single-phase LTP-MnBi alloy through peritectic reaction, because other phases are not easily avoided during the preparation process, and LTP MnBi phase can decompose at high temperature [6, 7]. Therefore, many researchers are devoted to obtain single-phase MnBi alloys. The MnBi alloys with highly pure LTP have been prepared by several methods, such as mechanical alloying, melt-spinning, sintering, and suction casting [8-11]. Element doping is also considered as another feasible way to optimize the magnetic performance of MnBi alloy. The influence of the partial substitution of Bi by rare earth elements on the magnetic properties of MnBi alloys is found to increase the coercivity, duing to the increase of magnetocrystalline anisotropic field and the grain size refinement [12]. Kharel *et al.* reported the disorder of MnBi melt spinning ribbons is caused by the addition of a third element, and explained the change of magnetic properties according to the competitive ferromagnetic and antiferromagnetic interactions [13]. The Curie temperature and the phase transformation temperature of $Mn_{55}Bi_{45}$ alloy increase with the Ga-doping [14]. Moreover, some works have been reported so far about doping other elements like Cr, Sn, Mg, Zr, Al, Cu and Ti to improve magnetic performance of MnBi alloys [15-18]. Yang *et al.* reported the addition of Fe element could enhance the coercivity of the MnBi-based alloy, and a high remanence ratio of 97.0 % was achieved in the $Mn_{55}Bi_{45}$-Fe (7.5 wt%) ball-milled ingot [19]. In this paper, the effects of Fe-doping on the microstructure and magnetic properties of $Mn_{55}Bi_{45-x}Fe_x$ (x = 0, 1, 3 and 5) ribbons are studied specifically.

*Corresponding author: Tel: +86-571-87676292
Fax: +86-571-28889526, e-mail: wuqiong@cjlu.edu.cn

2. Experimental

$Mn_{55}Bi_{45-x}Fe_x$ (x = 0, 1, 3 and 5) alloy ingots were synthesized by arc melting of manganese, bismuth and iron with high purity (> 99.9 %) in an argon atmosphere. Manganese flakes are placed at the bottom of the crucible due to the explosive nature of manganese. For the homogeneity of the ingot, the ingot should be melted for more than 5 times. In order to improve the interdiffusion of Mn and Bi, the ingots were annealed at the temperature of 573 K for about 24 h in the vacuum. The annealed ingots were then cut into small pieces. Small amounts of the $Mn_{55}Bi_{45-x}Fe_x$ (x = 0, 1, 3 and 5) alloy ingots were put in a quartz crucible with an orifice of 0.6 mm at the bottom. The alloy ingot in quartz crucible is preheated until the alloy is completely melted by induction in argon atmosphere, and then the molten metals were sprayed through the orifice by controlling argon pressure difference inside and outside quartz crucible onto a copper wheel with a surface velocity of 40 m/s. The $Mn_{55}Bi_{45-x}Fe_x$ (x = 0, 1, 3 and 5) melt-spun ribbons were annealed in vacuum at 523 K for 10 min.

The X-ray diffraction (XRD) with Cu-K_α radiation was used to analyze the phase composition of the samples prepared in the experiment. Differential scanning calorimeter (DSC) in the environment of argon atmosphere at a 40 K/min heating rate to 823 K was utilized to check the phase transformation process of samples. The microstructure of samples was observed by a transmission electron microscope (TEM). Vibrating sample magnetometer was used to test the hysteresis loops of samples at room temperature. Moreover, the hysteresis loops with various temperatures ranged from 273 K to 573 K were characterized by PPMS with 50 kOe applied field.
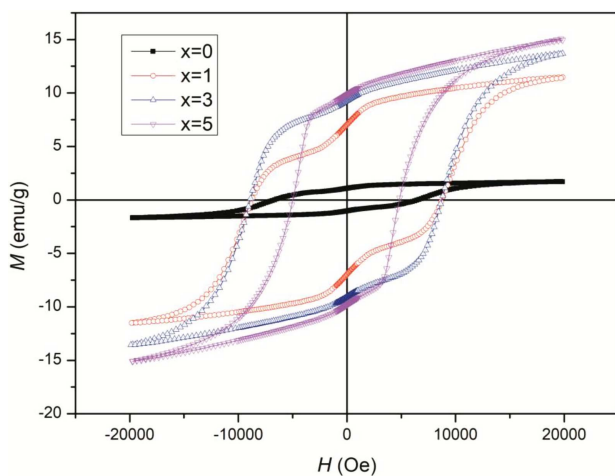
3. Result and Discussion

Figure 1 shows magnetic hysteresis loops of the as-spun $Mn_{55}Bi_{45-x}Fe_x$ (x = 0, 1, 3 and 5) ribbons. As can be seen from Fig. 1, The hysteresis loop with hard magnetic behavior is observed. It is indicated that the LTP hard magnetic phase is formed in the as-spun ribbons by melt-spinning process, which is similar to other reports [20]. The magnetization at the 20 kOe field of the as-spun Mn-Bi ribbons increase obviously by the doping of Fe element. The coercivity H_{cj} of the Mn-Bi-Fe ribbons first increase and then decrease with the increasing of Fe content. A high coercivity of more than 9 kOe is obtained.

The XRD patterns of the as-spun $Mn_{55}Bi_{45-x}Fe_x$ (x = 0, 1, 3, 5) ribbons are illustrated in the Fig. 2. The main phases of samples consist of LTP-MnBi, Bi, and tiny amount of Mn. There is no soft magnetic phase of α-Fe, which has high saturation magnetization. It indicates that the increase of magnetization in Fig. 1 is not caused by existence of α-Fe soft magnetic phase. The relative content of the LTP-MnBi can be characterized by the ratio of MnBi (101) peak to Bi (012) peak. With the addition of 1 at% Fe, the relative content of the LTP-MnBi in the as-spun samples increased from ~7.7 % to ~33.1 %, which leads to an increase of the magnetization at the 20 kOe field. The increase of LTP-MnBi resulted in the enhancement of the magnetization. However, due to the low content of the LTP-MnBi in the as-spun Mn-Bi ribbons, the M_s of the Mn-Bi-Fe melt-spun ribbons is not more than 15 emu/g.

The effects of Fe doping on the LTP-MnBi Formation is investigated by the DSC scanning. The relationship between the heat flow and temperature for $Mn_{55}Bi_{45-x}Fe_x$ (x = 0, 3) melt spun ribbons is shown in Fig. 3. According

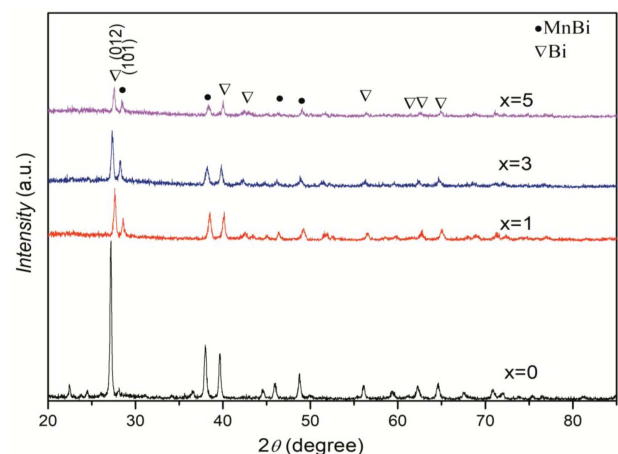**Fig. 1.** (Color online) Magnetic hysteresis loops of the as-spun $Mn_{55}Bi_{45-x}Fe_x$ (x = 0, 1, 3 and 5) ribbons.

Fig. 2. (Color online) XRD patterns of the as-spun $Mn_{55}Bi_{45-x}Fe_x$ (x = 0, 1, 3 and 5) ribbons.
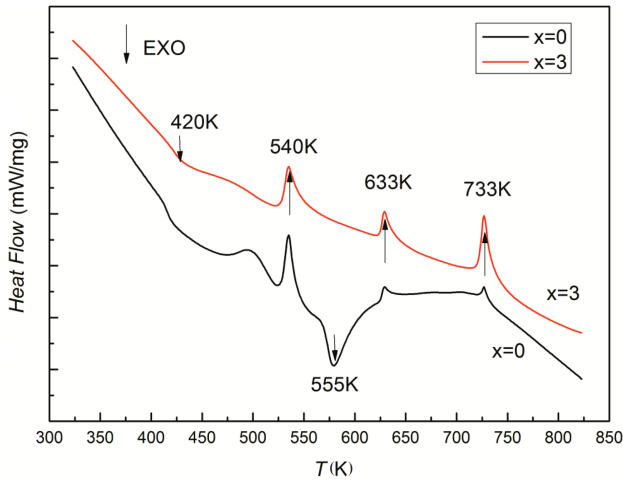
Fig. 3. (Color online) DSC scan of the $Mn_{55}Bi_{45-x}Fe_x$ (x = 0, 3) spun ribbons.

Table 1. The relative content of LTP MnBi for as-spun and annealed $Mn_{55}Bi_{45-x}Fe_x$ (x = 0, 1, 3 and 5) alloys.

	x = 0	x = 1	x = 3	x = 5
As-spun ribbons	7.7 %	33.1 %	35.2 %	31.5 %
Annealed ribbons	16 %	48.3 %	54.8 %	57.2 %

to the results, the x = 0 and x = 3 samples show small exothermic peak at 420 K which are considered as the crystallization of small fraction of ferromagnetic MnBi [21, 23]. The characteristic melting temperature of Bi is representing as the endothermic peak at 540 K which can be observed in both the x = 0 and x = 3 samples, in accordance with the XRD results. The endothermic peak of $Mn_{55}Bi_{45}$ sample at 490 K indicates the formation of LTP-MnBi. In the view of this peak means that the extra heat is needed and necessary to form LTP-MnBi. There is no peak could be found at 590 K in the x = 3 sample which indicates that the Fe doping in MnBi contributes directly to the formation of LTP-MnBi. According to the data, it is obvious that the addition of Fe is favor to the formation of LTP-MnBi. Other two endothermic peaks at
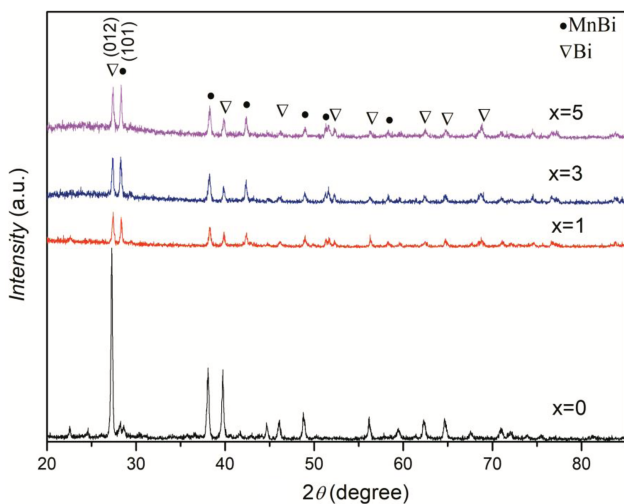
633 K and 730 K are consistent with the LTP to HTP transformation of MnBi and the peritectic decomposition of HTP. These results were also reported by other researches [24, 25].

The ribbons are annealed at 523 K for 10 min to greatly enhance the magnetic performance of Mn-Bi-Fe alloys. Fig. 4 shows the XRD patterns of the annealed $Mn_{55}Bi_{45-x}Fe_x$ (x = 0, 1, 3 and 5) spun ribbons. The composition of the main phase has not changed by the annealed treatment for all samples, but the intensity of the diffraction peak for LTP-MnBi are obviously enhanced after the annealed treatment. The relative content of LTP-MnBi for as-spun and annealed Mn-Bi-Fe alloys is list as Table 1. With the addition of Fe, the relative content of the LTP-MnBi in the annealed alloys increases from 16 % for x = 0 to 57.2 % for x = 5.

The magnetic hysteresis loops of the $Mn_{55}Bi_{45-x}Fe_x$ (x = 0, 1, 3 and 5) melt-spun ribbons after annealed at 523 K for 10 min are shown in Fig. 5. Heat treatment of the Mn-Bi melt-spun ribbons results in drastic changes in the magnetic properties, especially magnetization. As shown in the figure, the magnetization of the $Mn_{55}Bi_{45-x}Fe_x$ (x = 0, 1, 3 and 5) melt-spun ribbons has been improved after being annealed. It is because the diffusion of Mn and Bi in the annealing process promotes the formation of LTP MnBi. The maximum magnetization (45 emu/g) of $Mn_{55}Bi_{40}Fe_5$ melt-spun ribbons is achieved in our samples.
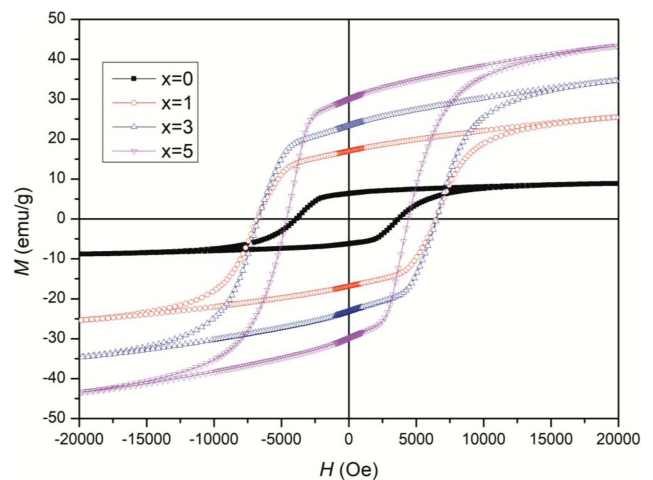

Fig. 4. (Color online) XRD patterns of the $Mn_{55}Bi_{45-x}Fe_x$ (x = 0, 1, 3 and 5) spun ribbons annealed at 523 K.

Fig. 5. (Color online) Magnetic hysteresis of the $Mn_{55}Bi_{45-x}Fe_x$ (x = 0, 1, 3 and 5) spun ribbons after being annealed.

The H_{cj} of the annealed alloys first increase and then decrease with the Fe content increasing. The maximum coercivity value of 7 kOe is obtained in the x = 1 and x = 3 samples. The change of H_{cj} may be related to the grain distribution and the exchange coupling interaction.

In order to understand dependence of coercivity on Fe content, the exchange coupling interaction between magnetic particles is characterized by using δM plot, which can be defined as $\delta M = m_d(H) - [1-2m_r(H)]$, where $m_r(H)$ is acquired after the application and subsequent removal of a direct field H and $m_d(H)$ is acquired after dc saturation in one direction and the subsequent application and removal of a direct field H in the reverse direction. For the assembly of uniaxial single-domain particle, nonzero δM is believed to be due to the particle inter-action for a magnet where the positive values of δM are due to exchange coupling interaction, while the negative values of δM are reasonably caused by the dipolar interaction [26, 27]. The positive δM-peak height reflects the strength of exchange coupling interaction, which is generally located at the field around coercivity [28]. Fig. 6 shows that the δM plots of the annealed x = 0, 1 and 5 alloy ribbons. A positive δM is observed in all the three samples, confirms the existence of exchange coupling interaction between magnetic particles. Evidently, compared to x = 1 sample, the larger positive δM value could be obtained in x = 5 alloy ribbon while the peak of the δM curve locates at lower field, which indicates that with the addition of 5 at% Fe, the exchange coupling interaction between LTP-MnBi magnetic particles increases and the coercivity decreases. The reduction of H_{cj} can be explain-ed by greater volume fraction of the ferromagnetic LTP and correspondingly smaller fraction of the magnetically insulating phases, favoring the exchange coupling between
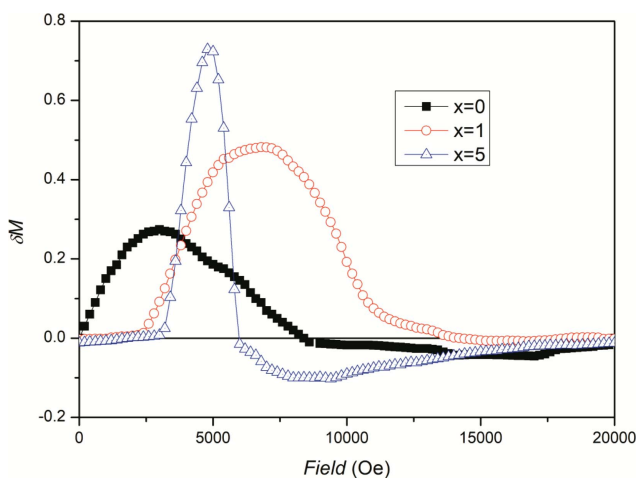
LTP-MnBi particles. The minimum peak of δM is observed and the peak locates at lowest field for x = 0 sample. It is consistent with the coercivity of magnetic hysteresis loop.

The microstructure of the annealed ribbons has been examined by TEM. Fig. 7(a-c) shows the microstructure of the $Mn_{55}Bi_{45-x}Fe_x$ (x = 0, 1 and 5) spun ribbons after
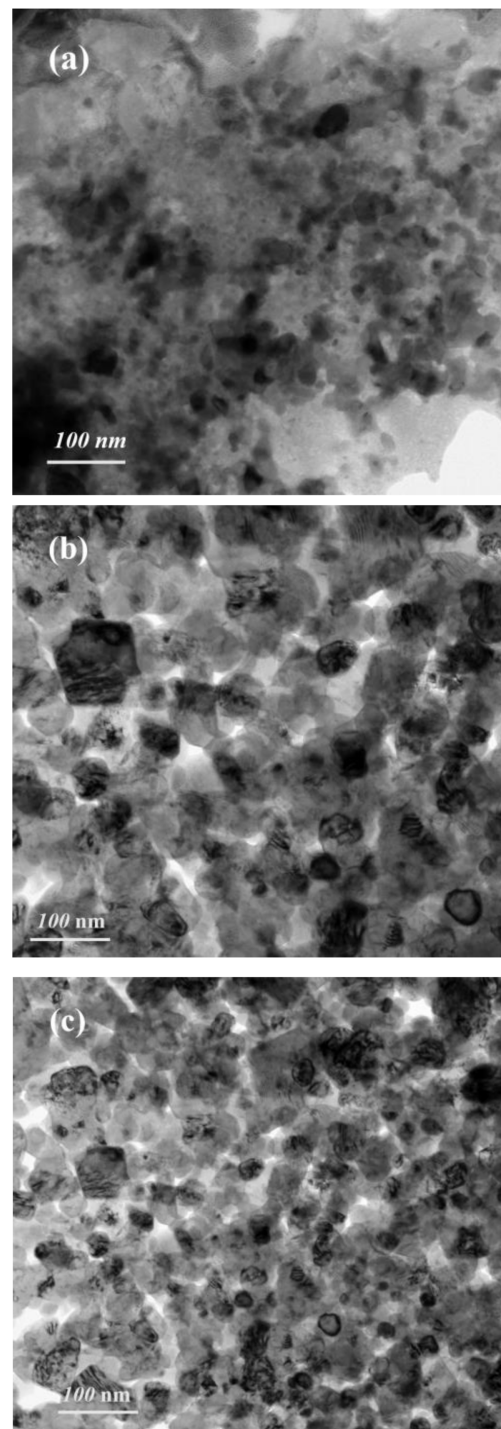

Fig. 7. TEM micrographs of $Mn_{55}Bi_{45-x}Fe_x$ (a) x = 0, (b) x = 1 and (c) x = 5 spun ribbons after being annealed.

Fig. 6. (Color online) δM plots for the $Mn_{55}Bi_{45-x}Fe_x$ (x = 0, 1 and 5) spun ribbons after being annealed.
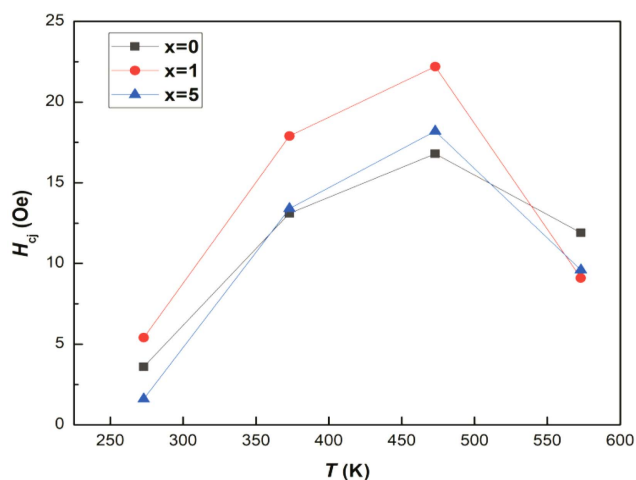
Fig. 8. (Color online) Hysteresis loops of the annealed $Mn_{55-x}Bi_{45-x}Fe_x$ (x = 0, 1 and 5) melt-spun ribbons at different temperature.

being annealed. Combined with the results of XRD, we infer that more LTP-MnBi is formed in the Fe-doped MnBi alloy compared with Fe-free alloy. Furthermore, the average grain size of x = 5 is about 10 nm, smaller than that of x = 1 (about 30 nm). The finer grain size leads to an enhancement exchange coupling with the addition of 5 at% Fe.

To study the dependence of coercivity on temperature for the annealed MnBi alloy melt-spun ribbons, magnetization measurements with different temperature have been carried out by PPMS with 50 kOe maximum magnetic field. Fig. 8 shows the hysteresis loops of the annealed $Mn_{55}Bi_{45-x}Fe_x$ (x = 0, 1 and 5) melt-spun ribbons, measured at elevated temperatures from 273 K to 573 K. It clearly shown in Fig. 7 that the coercivity increases with temperature in the range of 273 K to 573 K for all the three samples. The coercivity did not decrease until 473 K.The maximum coercivity values of 17 kOe, 22 kOe and 18 kOe are obtained at 473 K for x = 0, 1 and 5 samples, respectively. It is in an advantageous position for the high temperature performance of NdFeB magnets with a coercivity drops to 2 kOe at an elevated temperature of 473 K [29]. The positive temperature coefficient of coercivity of MnBi alloy system originates from its positive temperature coefficient of magnetocrystalline anisotropy [30].

4. Conclusions

The $Mn_{55}Bi_{45-x}Fe_x$ (x = 0, 1, 3 and 5) alloys have been synthesized by melt spinning technique. Some LTP-MnBi phases are found in the as-spun Mn-Bi-Fe ribbons, which possess an optimal coercivity of more than 9 kOe for x =

1 and x = 3 sample. The content of the LTP-MnBi is increased by annealing of the as-spun ribbons. The magnetization of the Fe-doped MnBi ribbons is much larger than the Fe-free samples after being annealing, indicating that the Fe addition is in favor of the pre-cipitation of the MnBi LTP in the annealing process. The dependence of coercivity H_{cj} on the Fe content can be explained by distribution of grain and their interaction. According to TEM images and δM plots, there is small amount of LTP MnBi and weak exchange coupling inter-action for x = 0 sample, the exchange coupling increases with the increase of LTP-MnBi for x = 1 sample, the strongest exchange coupling is founded in the x = 5 sample due to grain refinement. The maximum coercivity values of 17 kOe, 22 kOe and18 kOe have been obtained at 473 K for x= 0, 1 and 5 samples, respectively.

References

[1] T. Chen and E. Stutius, IEEE Trans. Magn. **10**, 581 (1974).
[2] B. W. Roberts, Phys. Rev. **104**, 607 (1956).
[3] E. Adams, W. M. Hubbard, and A. M. Syeles, J. Appl. Phys. **23**, 1207 (1952).
[4] J. Park, Y. K. Hong, J. Lee, W. Lee, S. G. Kim, and C. J. Choi, Metals **4**, 455 (2014).
[5] X. Guo, X. Chen, Z. Altounian, and J. O. Ström-Olsen, Phys. Rev. B **46**, 14578 (1992).
[6] N. V. Rama. Rao and G. C. Hadjipanayis, J. Alloys Compd. **616**, 319 (2014).
[7] T. Saito, R. Nishimura, and D. Nishio-Hamane, J. Magn. Magn. Mater. **49**, 9 (2014).
[8] J. Cui, J. P. Choi, E. Polikarpov, M. E. Bowden, W. Xie, G. Li, Z. Nie, N. Zarkevich, M. J. Kramer, and D. John-son, Acta Mater. **79**, 374 (2014).
[9] D. T. Zhang, P. F. Wang, M. Yue, W. Q. Liu, J. X. Zhang, A. S. Jennifer, and Y. Qiang, Rare Metals **35**, 471 (2016).
[10] W. Xie, E. Polikarpov, J. P. Choi, M. E. Bowden, K. Sun, and J. Cui, J. Alloys. Compd. **680**, 1 (2016).
[11] S. Kim, H. Moon, H. Jung, S. M. Kim, H. S. Lee, C. Y. Haein, and W. Lee, J. Alloys Compd. **708**, 1245 (2017).
[12] P. Kharel, V. R. Shan, X. Z. Li, W. Y. Zhang, R. Skomski, J. E. Shield, and D. J. Sellmyer, J. Appl. Phys. **46**, 095003 (2013).
[13] P. Kharel, X. Z. Li, V. R. Shah, N. Al-Aqtash, K. Tarawneh, R. F. Sabirianov, R. Skomski, and D. J. Sell-myer, J. Appl. Phys. **111**, 07E326 (2012).

[14] Y. Yang, J. W. Kim, P. Z. Si, H. D. Qian, Y. Shin, X. Y. Wang, J. Park, O. L. Li, Q. Wu, H. L. Ge, and C. J. Choi, J. Alloy Compd. **769**, 813 (2018).

[15] T. X. Nguyen, H. V. Pham, and V. V. Nguyen, Physica B: Condens. Matter. **552**, 190 (2019).

[16] V. V. Ramakrishna, S. Kavita, and R. Gautam, J. Magn. Magn. Mater. **458**, 23 (2018).

[17] E. S. Olivetti, C. Curcio, and L. Martino, J. Alloy Compd. **543**, S270 (2015).

[18] M. Sagawa, S. Fujimori, M. Togawa, and Y. Matsuura, J. Appl. Phys. **55**, 2083 (1984).

[19] Y. Yang, J. T. Lim, H. D. Qian, J. Park, J. W. Kim, O. L. Li, and C. J. Choi, J. Alloys Compd. **855**, 157312 (2021).

[20] A. M. Gabay, G. C. Hadjipanayis, and J. Cui, J. Alloys Compd. **792**, 77 (2019).

[21] A. Kritika, C. Nithya, and S. Nidhi, Appl. Phys. A **125**, 870 (2019).

[22] S. Saha, R. T. Obermyer, B. J. Zande, V. K. Chandhok, S. Simizu, S. G. Sankar, and J. A. Horton, J. Appl. Phys. **91**, 8525 (2002).

[23] Y. B. Yang, X. G. Chen, S. Guo, A. R. Yan, Q. Z. Huang, M. M. Wu, D. F. Chen, Y. C. Yang, and J. B. Yang, J. Magn. Magn. Mater. **330**, 106 (2013).

[24] X. Guo, A. Zaluska, Z. Altounian, and J. O. Strom-Olsen, J. Mater. Res. **5**, 2646 (1990).

[25] X. Guo, A. Zaluska, Z. Altounian, and J. O. Strom-Olsen, J. Appl. Phys. **69**, 6067 (1991).

[26] E. P. Wohlfarth, J. Appl. Phys. **29**, 595 (1958).

[27] P. E. Kelly, K. O. Grady, P. I. Mayo, and R. W. Chantrell, IEEE Trans. Magn. **25**, 3881 (1989).

[28] H. W. Zhang, C. B. Rong, X. B. Du, J. Zhang, S. Y. Zhang, and B. G. Shen, Appl. Phys. Lett. **82**, 4098 (2003).

[29] W. Q. Liu, C. Chang, M. Yue, J. S. Yang, D. T. Zhang, J. X. Zhang, and Y. Q. Liu, Rare Metals **36**, 718 (2017).

[30] M. Yue, J. X. Zhang, and Y. F. Xiao, IEEE Trans. Magn. **39**, 3551 (2003).